Article

All-Photochemical Rotation of Molecular Motors with a Phosphorus Stereoelement

Gregory B. Boursalian, Eise R. Nijboer, Ruth Dorel, Lukas Pfeifer, Omer Markovitch, Alex Blokhuis, and Ben L. Feringa*

Cite This: *J. Am. Chem. Soc.* 2020, 142, 16868−16876

Read Online

ACCESS | Metrics & More | Article Recommendations | Supporting Information

ABSTRACT: Unidirectional molecular rotation based on alternating photochemical and thermal isomerizations of overcrowded alkenes is well established, but rotary cycles based purely on photochemical isomerizations are rare. Herein we report three new second-generation molecular motors featuring a phosphorus center in the lower half, which engenders a unique element of axial chirality. These motors exhibit unusual behavior, in that all four diastereomeric states can interconvert solely photochemically. Kinetic analysis and modeling reveal that the behavior of the new motors is consistent with all-photochemical unidirectional rotation. Furthermore, X-ray crystal structures of all four diastereomeric states of two of these new motors were obtained, which constitute the first achievements of crystallographic characterization of the full 360° rotational cycle of overcrowded-alkene-based molecular motors. Finally, the axial phosphorus stereoelement in the phosphine motor can be thermally inverted, and this epimerization enables a "shortcut" of the traditional rotational cycle of these compounds.
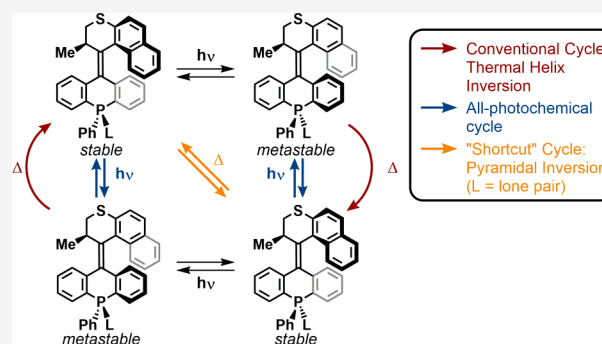
INTRODUCTION

The complex artificial molecular machines of the future will be built from components with tailored properties suited to their particular function.[1] Thus, there is a need for new functional molecules, such as molecular motors and switches, with novel and varied attributes for molecular engineers to draw from in their designs. Overcrowded-alkene-based molecular motors, which operate through a unidirectional rotary cycle consisting of alternating photochemical and thermal steps (Figure 1A),[2] are an appealing class of actuators for such machines because of their ability to convert light energy into mechanical force at the nanoscale. The design and study of a wide range of motors utilizing this operating principle have enabled the engineering of functional systems including dynamic metal−organic and covalent frameworks,[3] hierarchical supramolecular assemblies with artificial muscle-like function,[4] and liquid crystals with rotating helicity capable of mechanically rotating microscale objects.[5]

Barely explored, however, are molecular motors that rotate through a unidirectional sequence consisting solely of photochemical steps. Aside from the fundamental challenge of orchestrating consecutive photoisomerization reactions so as to form a rotary cycle, such all-photochemical motors could have practical advantages over traditional molecular motors. For example, their rotation is limited only by the light they absorb and the quantum yield of their photoreactions, and does not depend in the same way on the ambient temperature. So far, the only known example of an all-photon molecular motor is one based on the hemithioindigo chromophore, reported by Dube and co-workers in 2018.[6]

Here, we report the design, synthesis, and properties of a new second-generation[7] molecular motor **1** with a Lewis-basic phosphorus atom embedded in the lower half. Also disclosed are the gold(I) complex **2** ligated by **1**, and the phosphine oxide derivative **3** (Figure 1B). These motors feature an element of axial chirality[8] that is unprecedented in molecular motors, engendered by the tetrahedral phosphorus atom lying on the motor's axis of rotation. Unexpectedly, we have found that all four of the diastereomers of motors **1**−**3** can be interconverted *solely photochemically*, which stands in contrast to the relatively clean-cut photochemical double-bond isomerization typical of overcrowded alkenes. We show that photochemical interconversion of all four states of overcrowded-alkene-based rotary motors is possible, and we provide strong evidence that it can be considered all-photochemical unidirectional rotation, in that there is a predominant sequence of isomerizations that mimics
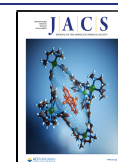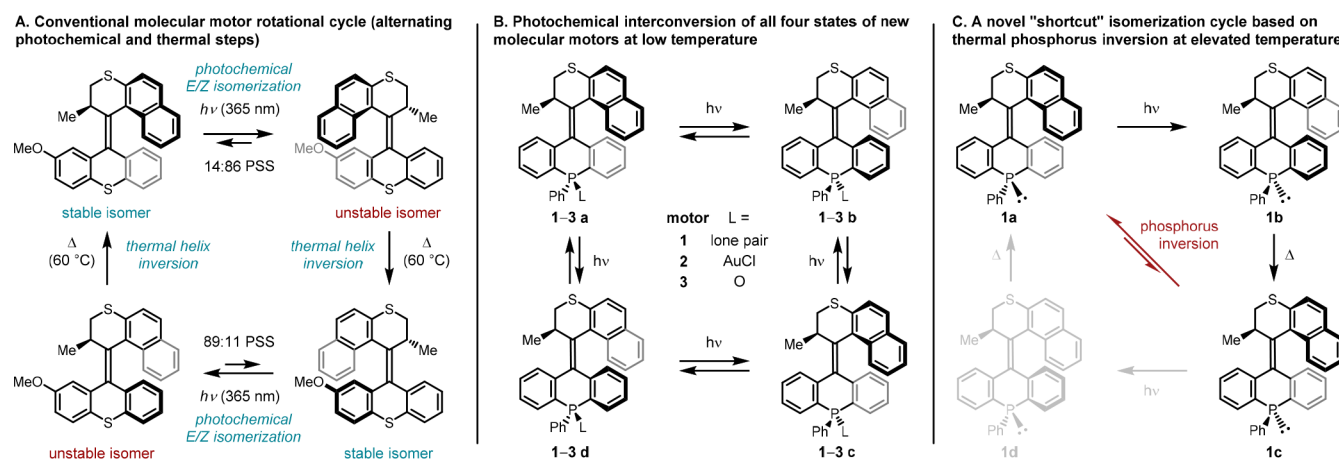
Figure 1. (A) Conventional rotary cycle of a second-generation molecular motor, consisting of alternating photochemical and thermal steps. (B) New phosphine-based molecular motors **1−3**, which are capable of accessing all four diastereomeric states photochemically, even at low temperatures. (C) A unique isomerization cycle of phosphine motor **1** taking advantage of pyramidal inversion at phosphorus, which occurs at elevated temperatures.

that of the conventional rotary cycle of alternating thermal and photochemical steps.

Also demonstrated herein is a unique isomerization cycle of the free phosphine motor **1** in particular (Figure 1C). The stereochemical lability of the phosphorus center allows the configuration of the axial stereoelement to be inverted, which converts one isomer of stable helicity (**1c**) directly into the other (**1a**), thereby bypassing half the conventional isomerization cycle of molecular motors.

Enabling our studies are a number of unique features of the new motors **1−3**. First, their unstable states have barriers to thermal helix inversion (THI) large enough that the process can be frozen out at low temperature, so that study of the photochemical processes is not convoluted by superimposed thermal reactions. Furthermore, the phosphorus-31 nucleus provides an ideal handle for monitoring the evolution of the complex photochemical reaction network by NMR. Because of the central position of the phosphorus atom along the axis of rotation, each of the four diastereomers of motors **1−3** has a distinct ^{31}P resonance.

RESULTS AND DISCUSSION

Synthesis of New Motors 1−3. Our synthesis of the new phosphine motor **1** (Scheme 1) begins from known acrido-phosphine derivative **4**.[9] Heating **4** with 2.5 equiv of Lawesson's reagent results in deoxysulfurization of both the ketone and phosphine oxide groups, giving the new thioketone **5**. Barton−Kellogg coupling of **5** with diazoalkane **6**, generated in situ by a standard method,[7b] gives thiirane **7** as a mixture of diastereomers. Desulfurization of **7** with hexamethylphosphor-triamine yields the phosphine motor **1** as a mixture of diastereomers **1a**:**1c** = 77:23, differing in their configuration at phosphorus. The diastereomers **1a** and **1c** do not interconvert at room temperature; they are separable by careful chromatog-raphy, and can be obtained essentially diastereomerically pure (>99% for **1a**, >96% for **1c**). Starting from **1a** and **1c**, gold(I) phosphine complexes **2a** and **2c** were obtained through ligand substitution of ClAu(SMe$_2$). Furthermore, oxidation of **1a** and **1c** with hydrogen peroxide proceeds chemoselectively to yield the corresponding phosphine oxides **3a** and **3c**. These derivatizations of **1a** and **1c** proceed with complete stereo-chemical fidelity, and the relative stereochemistry of each

Scheme 1. Synthesis of Motors 1−3
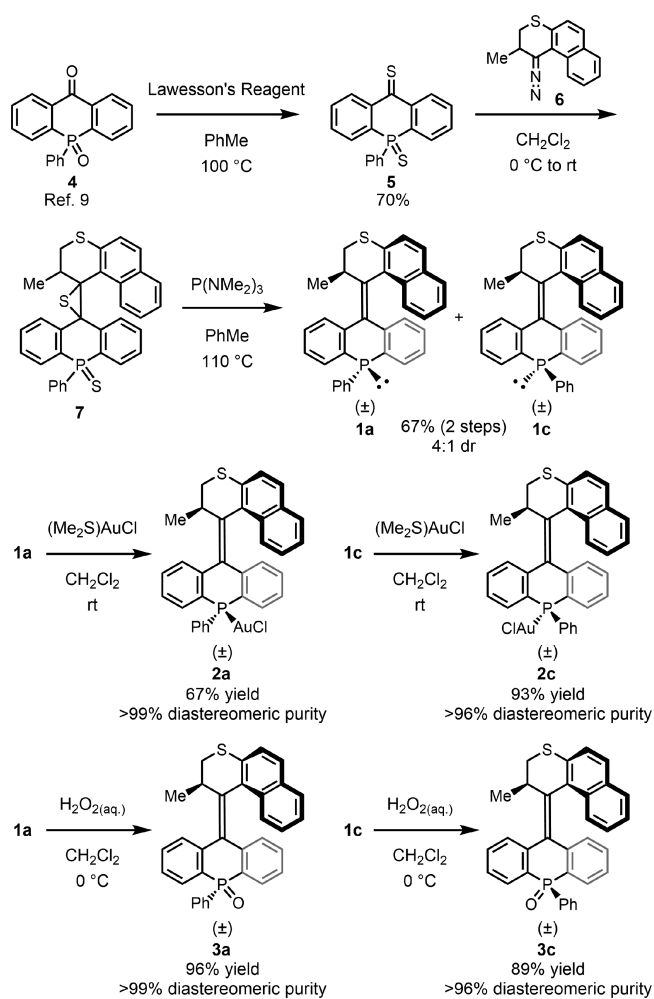
diastereomer was definitively established by X-ray crystallog-raphy (vide infra).

The phosphine motor **1** and its derivatives **2** and **3** possess a unique stereoelement, unprecedented in molecular motors; the tetrahedral phosphorus atom lies on the axis of rotation of the motor (the central alkene double bond), which introduces an element of axial chirality of the kind encountered in alkylidene-
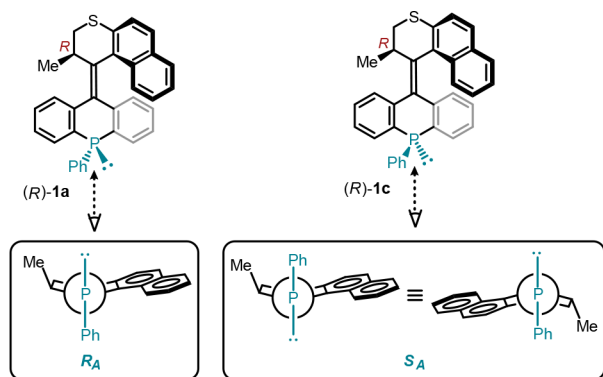
Figure 2. Illustration of the axial chirality engendered by the tetrahedral phosphorus center of motors **1**−**3**, using (R)-**1a** and (R)-**1c** as an example.

Table 1. Photostationary State Ratios of 2a−d as a Function of Wavelength[a]

wavelength	2a	2b	2c	2d
340 nm	27	51	8	14
365 nm	17	70	3	10
395 nm	3	97	0	<1

[a]Irradiation conducted in d_8-THF at −20 °C starting from **2a**. PSS ratios measured by ^{31}P NMR.

Table 2. Photostationary State Ratios of 3a−d as a Function of Wavelength[a]

wavelength	3a	3b	3c	3d
365 nm	13	75	5	7
385 nm	4	85	3	8
405 nm	3	88	<1	9

[a]Irradiation conducted in d_8-THF at −50 °C starting from **3a**. PSS ratios measured by ^{31}P NMR.

cycloalkanes (Figure 2).[8,10] The configuration of this stereoelement can be inverted by one half-turn of the motor, and as such, this axial chirality constitutes a unique means of desymmetrizing the lower half of the motor, which is normally accomplished by placing a substituent on one or the other side of the lower half.

Photochemical Behavior of Motors 1−3. Motors **1**, **2**, and **3** fit the typical pattern of second-generation motors, in that each has four diastereomeric states, two of which are metastable and convert to their thermodynamically more stable counterparts through a thermally activated helix inversion (THI), as shown in Figure 1A. For a typical motor, irradiation of a stable diastereomer results in double-bond isomerization to an isomer with a metastable helix configuration, establishing a photostationary state (PSS) of the two isomers. However, investigation of the photochemical isomerization of motors **1**−**3** revealed a completely unexpected departure from this clean-cut photochemical behavior.

Irradiation of either stable state of **1**−**3** leads to a four-component PSS consisting of all possible diastereomeric states. Tables 1 and 2 give the composition of PSS for motors **2** and **3**, respectively, as a function of wavelength. For both motors, higher wavelengths increasingly favor the metastable isomers **2b** and **3b**, to the point where these isomers are present almost exclusively at 395 and 405 nm, respectively. These irradiation experiments were conducted at low temperature (−20 °C for **2**
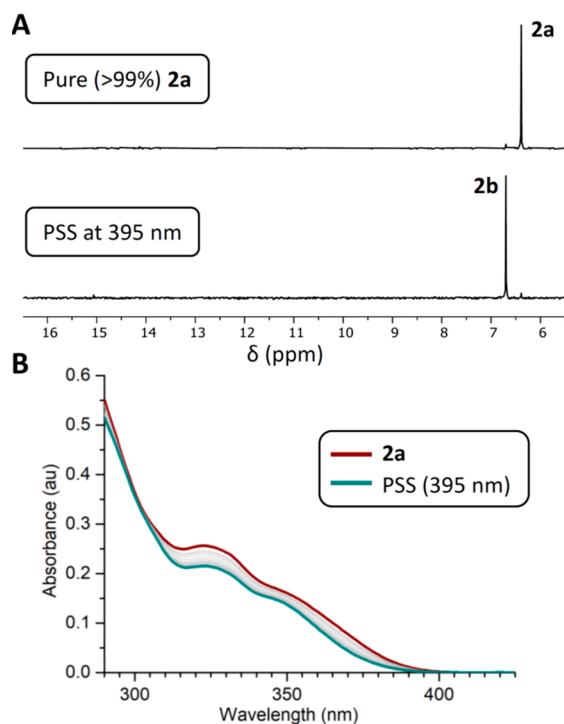

Figure 3. Pure **2a** and the PSS mixture after irradiation at 395 nm (−20 °C) as observed by (A) ^{31}P NMR spectroscopy and (B) UV/vis spectroscopy.

and −50 °C for **3**) at which the rate of THI is negligible, and the ratio of the four species remained constant when irradiation was suspended. Therefore, the processes giving rise to all four diastereomers must be solely photochemical, rather than a mixture of thermal and photochemical reactions. Figure 3 depicts the starting point and PSS of irradiation of **2a** with 395 nm as followed by ^{31}P NMR and UV/vis spectroscopy. The enantiomers of phosphine oxide motor **3a** could be separated by chiral supercritical fluid chromatography, and the absolute configuration of the (S)-enantiomer was determined by X-ray diffraction (vide infra). Figure 4 shows **3a** and the PSS mixture arising from irradiation at 405 nm by ^{31}P NMR, UV/vis, and circular dichroism spectroscopy with (S)-**3a**. The CD spectra show the expected sign-inversion of Cotton effects moving from (S)-**3a** to the PSS composed predominantly of (S)-**3b**.[7b]

Photochemical study of the parent phosphine motor **1** is complicated by its rapid reaction with oxygen upon UV irradiation. This precludes the use of our standard apparatus for NMR monitoring, from which it is impossible to exclude oxygen to a sufficient degree. Clean photoisomerization of **1a** and **1c** was accomplished by irradiation of a sample of each isomer in rigorously degassed d_8-toluene solution, prepared through several freeze−pump−thaw cycles in a J-Young NMR tube. Irradiation at 365 nm of either stable isomer yielded the same mixture composed mainly of **1b** (**1a:b:c:d** = 4:92:3:<1), consistent with the behavior of **2** and **3**.

Though such atypical photochemical behavior has been observed once before in a second-generation motor,[11] the question of whether it represents a specific predominant sequence of isomerizations, and if such a sequence can be considered unidirectional rotation, has never been addressed. Recently, the group of Dube has elegantly shown that a hemithioindigo-based alkene does in fact undergo a "photon-only" isomerization sequence that can be considered unidirec-
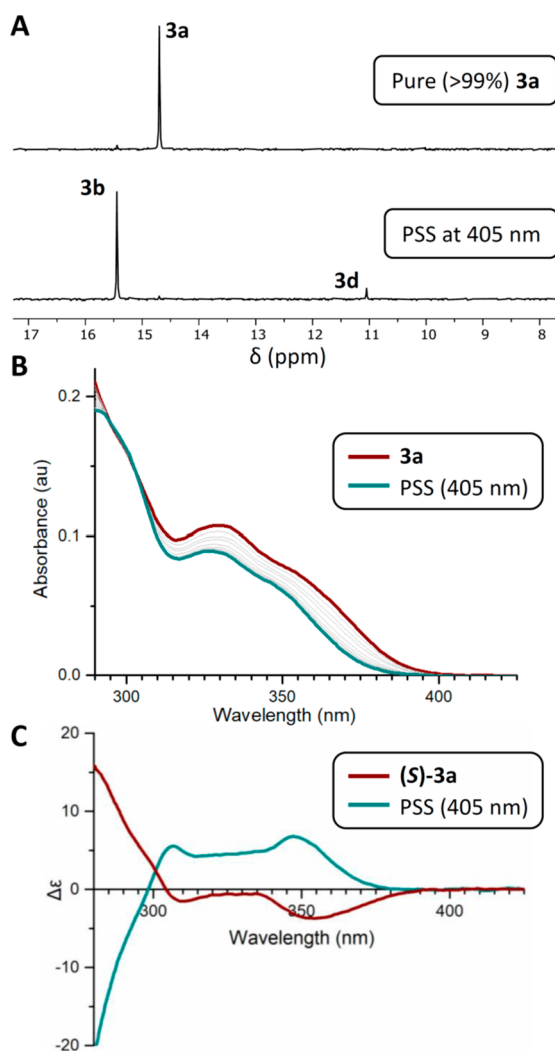
Figure 4. Pure **3a** and the PSS mixture after irradiation at 405 nm (−50 °C) as observed by (A) ^{31}P NMR spectroscopy, (B) UV/vis spectroscopy, and (C) CD spectroscopy from enantiopure (*S*)-**3a**.

Figure 5. Photokinetic profiles of approach to PSS from (A) **2a** irradiated with 395 nm at −20 °C, (B) **2c** irradiated with 395 nm at −20 °C, (C) **3a** irradiated with 405 nm at −50 °C, and (D) **3c** irradiated with 405 nm at −50 °C. In the runs starting from **2a** and **3a** (panels A and C, respectively), isomers **2c** and **3c** remained below the detection limit throughout the run.

tional rotation. This was established through Markov chain analysis of the absolute rates (derived from individually measured quantum yields) for all of the possible isomerizations.[6] Such an analysis is not possible in our case because unlike Dube's motor, only two of the four diastereomers (**a** and **c**) of motors **1**−**3** are thermally stable and isolable.[12]

Nevertheless, we were able to exploit two key features of our system to gain insight into the *relative* rates of the various processes at play. First, because the PSS of photoisomerization of motors **2** and **3** can be pushed to a single predominant isomer (**2b** and **3b**) through the choice of wavelength, the photokinetic profile of approach to these end states can be especially revealing. Second, each diastereomer of **2** and **3** presents a single, distinct phosphorus resonance, allowing the processes to be accurately followed by ^{31}P NMR spectroscopy. Samples of **2a** and **2c** in d_8-THF were irradiated at 395 nm through a fiber-coupled LED while inserted in an NMR probe at −20 °C. Under these conditions, **2a** appeared to convert directly to **2b**, with small amounts (<2%) of **2d** appearing as the PSS was approached (Figure 5A); thus, the dominant photoisomerization of **2a** appears to be double-bond isomerization to form **2b**, with subsequent transformations giving rise to a small steady-state concentration of **2d**.
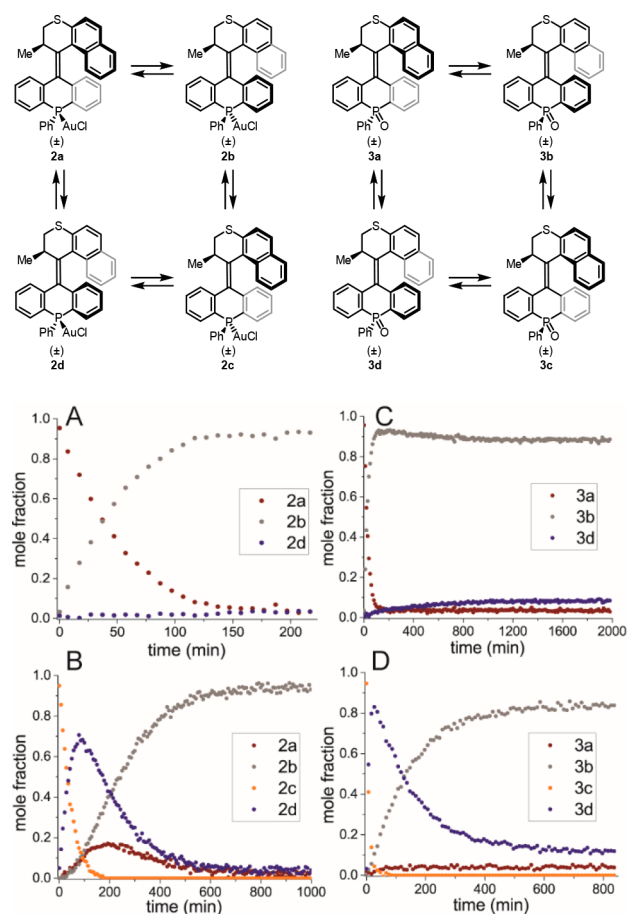
In contrast, when **2c** is irradiated under the same conditions, **2b** is not formed directly, but rather as the product of an apparent sequence of isomerizations involving **2d** and **2a** as intermediates (Figure 5B). Similar to the case of **2a**, the most rapid transformation of **2c** is double-bond isomerization, yielding **2d** as the first intermediate; thus, in the initial phase, the concentration of **2c** falls rapidly, while the concentration of **2d** rises to a maximum of ∼70% of the mixture. Subsequently, **2a** builds up and reaches its own maximum as **2d** is consumed. Then, the concentration of **2a** declines after its peak, while **2b** assumes its status as nearly the sole isomer present at PSS. Note additionally the sigmoidal shape of the curve for **2b**, which indicates a lag time in its formation. Overall, this time course has the familiar and classic profile of a series of consecutive reactions,[13,14] pointing to the sequence **2c**-**2d**-**2a**-**2b** as the predominant trajectory of the system. This sequence corresponds to a net unidirectional rotation of the motor *exclusively through photochemical isomerization steps*.

The photokinetic behavior of oxide motor **3** is similar in several respects. Irradiation of the stable isomer **3a** at 405 nm (d_8-THF, −50 °C) apparently yields **3b** directly (Figure 5C) through double-bond isomerization, after which the concentration of **3b** approaches its lower PSS concentration asymptotically. The approach of the system to PSS starting from **3c** is qualitatively similar to the behavior of **2c** (Figure 5D); initial
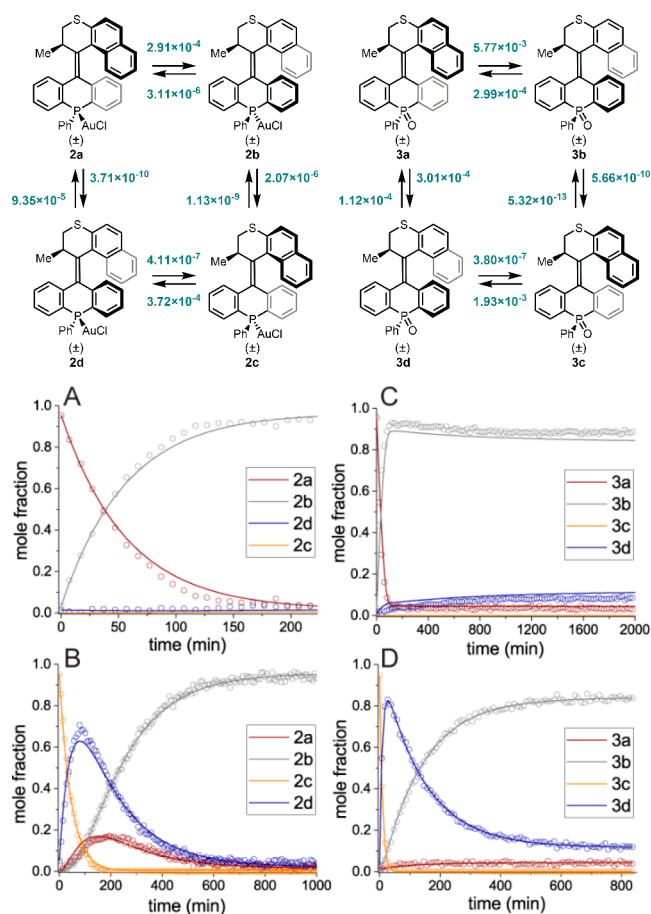
Figure 6. Optimized kinetic models and simulated time courses (solid lines) overlaid with experimental photokinetic data (open circles) starting from **2a** (A), **2c** (B), **3a** (C), and **3c** (D).

Table 3. Rates and Activation Parameters for Thermal Helix Inversion of 1b, 2b, 2d, 3b, and 3d[a]

metastable compound	product	$t_{1/2}$ (25 °C, h)	$\Delta G^{\ddagger}$ (25 °C, kcal/mol)
1b	**1c**	37.9	24.68 ± 0.05
2b	**2c**	30.3	24.54 ± 0.10
2d	**2a**	12.1	24.0 ± 0.08
3b	**3c**	5.4	23.53 ± 0.02
3d	**3a**	15.2	24.14 ± 0.08

[a]Rates determined by ^{31}P and ^{1}H NMR monitoring of THI in d_8-toluene (**1b**) or d_8-THF (all others) at 25−55 °C (see Supporting Information for details).

rapid conversion to **3d** implicates photochemical double-bond isomerization as by far the fastest initial process. However, as **3d** is consumed, no clear maximum is observed for **3a**; instead, its concentration initially rises and then remains level, which implies a kinetic steady state.

Kinetic Modeling. To glean more quantitative insight into the reaction trajectories depicted in Figure 5, and to test whether the observed trajectories can really be explained by a predominantly unidirectional cyclic isomerization sequence, we have employed the techniques of reaction network modeling. We considered a model involving the eight possible isomerizations around the periphery of the square depicted in Figure 1B; that is, interconversion of isomers **a** and **b**, **b** and **c**, **c** and **d**, and **d** and **a**. The transformations of motors **2** and **3** appear to be well-approximated as systems of first-order reactions, so we have

considered them as such, and assumed a constant photokinetic factor in our models.[15,16]

Figure 6 depicts the optimized models and their predicted trajectories, overlaid on the observed time courses. The fitting procedure was applied to the feature-rich time courses starting from **2c** and **3c**, and in both cases converged on a model that reproduces the observed concentration−time curves for all species very well. The measured time courses starting from **2a** and **3a** pose an important test for our optimized models; if the models simulated from these different initial conditions reproduce the measured data, it would serve as independent validation. Indeed, the model reproduces the shape of the curves quite well, though the simulations appear to converge slightly faster or slower than the measured data. This can be accounted for by the inconsistent light intensity reaching the sample between different experiments, which cannot easily be standardized with our fiber optic NMR irradiation apparatus.

The conventional rotary cycle involving THI implies a sequence proceeding alternately through stable and less-stable states; in principle, an all-photochemical isomerization manifold could involve direct interconversion of one stable state into another, or one metastable state into another. The models depicted in Figure 6 do not consider interconversion of isomers **b** and **d**, or **a** and **c**, which would involve an extreme geometric change within a single photochemical step. We cannot rule out with the current data whether these transformations are feasible or contribute at all to the overall kinetic behavior of **2** and **3**. However, our experimental data and modeling indicate that direct interconversions of **b** and **d** or **a** and **c** is not involved. Analytical treatment of the photokinetics of motors **2a** and **2c** can also rule out acyclic networks for **2**, because they cannot accommodate the observed features of the time courses (see Supporting Information).

Rates of Thermal Helix Inversion. Kinetic barriers and half-lives at room temperature for THI of unstable motors **1b**, **2b**, **2d**, **3b**, and **3d** are given in Table 3 (see Supporting Information for measurement details). The activation parameters for these processes are within the normal range for second-generation motors in which the alkenes are flanked by two six-membered rings.[7b] The room-temperature rate constants, which correspond to the maximum rate of rotation under ideal irradiation conditions, range from 1.8×10^{-2} to 1.3×10^{-1} s^{-1}. Importantly, the rates for all of these thermal processes are far too small to play any role in the photoisomerization studies at low temperature described above.

Crystallographic Characterization of 2 and 3. The gold-complexed motors **2** and phosphine oxide motors **3** crystallize readily. This has enabled, for the first time, the *crystallographic characterization of all four isomers of members of this class of molecular motors*. Previously, only two second-generation motors have been crystallized in a metastable helix configuration,[7,17] and only one of these two has the central double bond flanked by two six-membered rings as in **1**−**3**.[7] No overcrowded-alkene-based molecular motor of the first-, second-, or third-generation types pioneered by our group has ever been crystallized in all of the diastereomeric states constituting its rotary cycle.[18] Our crystallization of compounds **2a**−**d** and **3a**−**d** *triples* the number of structurally characterized metastable second-generation motor isomers, greatly increasing the structural information available on these strained compounds.

The compounds of stable helix configuration (**2a**, **2c**, **3a**, and **3c**) were easily crystallized from dichloromethane/pentane
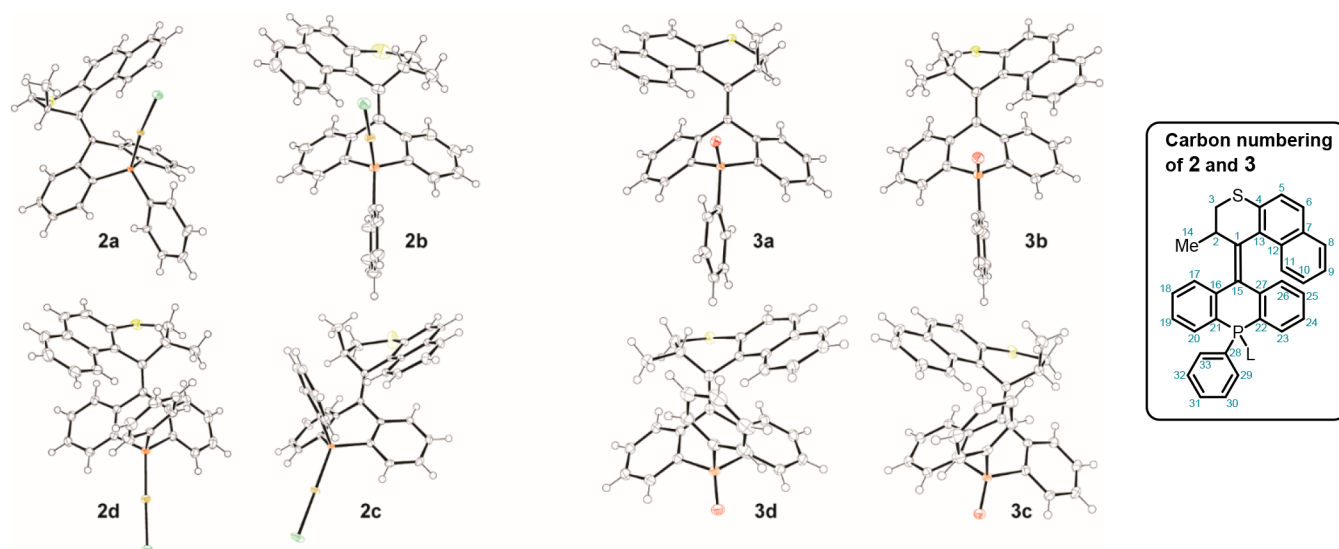
Figure 7. X-ray structures of gold complexes **2a–d** and phosphine oxides **3a–d**. Thermal ellipsoids at 50% probability level. Co-crystallized solvent molecules omitted for clarity.

Table 4. Selected Bond Metrics for Compounds 2a–d and 3a–d[a]

	2a	2b	2c	2d	3a	3b	3c	3d
C(1)–C(15)	1.350(6)	1.349(5)	1.352(4)	1.351(4)	1.350(3)	1.349(3)	1.352(3)	1.353(2)
$\Phi_{2\text{-}1\text{-}15\text{-}16}$	−0.7(8)	−1.2(6)	0.5(5)	−3.4(5)	3.1(3)	2.3(3)	−1.9(4)	0.2(2)
$\Phi_{13\text{-}1\text{-}15\text{-}27}$	−2.3(8)	−5.2(6)	4.7(5)	−6.7(4)	−0.2(3)	8.0(3)	2.0(4)	−5.4(2)
twist angle Φ_T	1.5(6)	3.2(4)	2.6(4)	5.1(3)	1.7(2)	5.2(2)	2.0(3)	2.8(1)
helical pitch	4.682(3)	4.328(2)	4.2445(15)	4.3768(15)	4.2493(12)	4.0098(10)	4.3414(14)	4.2115(8)
∠C(2)–C(1)–C(13)	112.8(3)	106.6(3)	111.1(2)	107.3(2)	113.36(18)	107.28(15)	112.37(18)	107.56(11)
∠C(2)–C(1)–C(15)	124.9(4)	128.7(3)	123.9(2)	131.0(2)	123.69(19)	129.81(17)	124.9(2)	130.28(13)
∠C(13)–C(1)–C(15)	122.3(4)	124.7(3)	124.9(3)	121.6(2)	122.89(19)	122.90(17)	122.6(2)	122.06(12)
sum	360.0(6)	360.0(5)	359.9(4)	359.9(4)	359.9(3)	359.99(28)	359.9(3)	359.90(21)
∠C(16)–C(15)–C(27)	112.7(3)	113.1(3)	113.1(2)	112.1(2)	112.41(18)	113.67(15)	113.71(18)	113.27(12)
∠C(16)–C(15)–C(1)	123.5(4)	125.1(3)	124.1(3)	126.7(2)	124.14(19)	125.16(17)	124.1(2)	125.99(13)
∠C(27)–C(15)–C(1)	123.8(4)	121.7(3)	122.9(2)	121.1(2)	123.44(19)	121.06(16)	122.2(2)	120.73(13)
sum	360.0(6)	359.9(5)	360.1(4)	359.9(4)	359.99(32)	359.89(28)	360.0(3)	359.99(22)
folding angle Φ_F	120.6(2)	132.87(18)	129.24(14)	123.30(12)	121.62(10)	133.79(9)	126.97(12)	132.22(7)
P–Au	2.2316(11)	2.2266(9)	2.2277(7)	2.2274(7)				
∠P–Au–Cl	172.99(5)	178.22(3)	179.56(3)	176.01(3)				
P=O					1.4949(16)	1.4921(13)	1.4877(16)	1.4874(10)

[a]All data collected at 100(2) K. $\Phi_{w\text{-}x\text{-}y\text{-}z}$ denotes the dihedral angle between the two planes defined by atoms w-x-y and x-y-z. The twist angle Φ_T is defined as the average of $\Phi_{2\text{-}1\text{-}15\text{-}16}$ and $\Phi_{13\text{-}1\text{-}15\text{-}27}$. The helical pitch is defined as the distance between the centroids of rings C(7–12) and C(22–27). The folding angle Φ_F is defined as the dihedral angle between the two average planes of rings C(16–21) and C(22–27). Bonds are given in angstroms and angles in degrees.
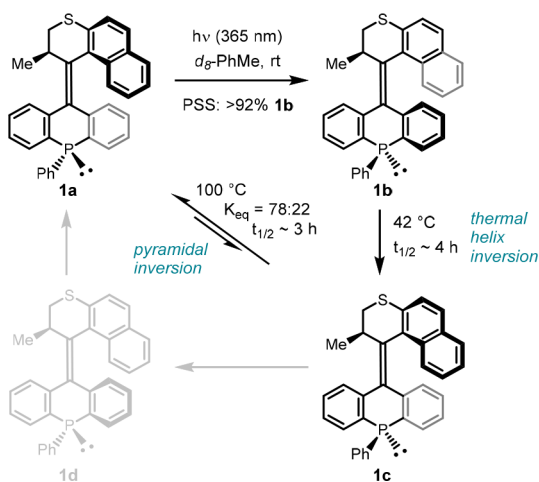
solvent mixtures. Metastable compounds **2b** and **3b** were crystallized from the photostationary mixtures generated through irradiation at 395 and 405 nm, respectively, and **2d** and **3d** were crystallized from mixtures enriched in these isomers, prepared by timed irradiation of **2c** and **3c**, respectively. The irradiations were conducted in THF solution, after which the solvent was removed, and the residue was re-dissolved in dichloromethane, then either layered with pentane or allowed to stand in a sealed chamber under pentane vapors.

ORTEP representations of compounds **2a–d** and **3a–d** are shown in Figure 7, and selected metrics are given in Table 4. We discuss here some noteworthy structural features.[19] The length of the central double bond of all eight compounds is almost invariant, each alkene deviating from the average of 1.351 Å by at most 0.002 Å. In all eight structures, both carbon atoms of the central alkene are very close to ideal planarity, as indicated by the sum of their bond angles, which in all cases falls between 359.9° and 360.1°.

Inspection of the individual alkene bond angles, however, reveals a significant in-plane distortion associated with the unstable helix configuration. In the more-stable diastereomers, each olefinic carbon has a somewhat contracted endocyclic C(2)–C(1)–C(13) bond angle (112.0° on average), while the exocyclic bond angles C(2)–C(1)–C(15) and C(13)–C(1)–C(15) are each expanded in roughly equal measure (124.4° and 123.6° on average, respectively). All four of the less-stable

Scheme 2. "Shortcut" Cycle of Motor 1 through Phosphorus Inversion

measured by the twist angle Φ_T (see caption of Figure 7 for definition). Intriguingly, the twist angle in the less-stable diastereomers appears to correlate with their rate of THI (Table 3); alkene **2d** ($\Phi_T = 5.1(3)°$) is more twisted than **2b** ($\Phi_T = 3.2(4)°$), and is correspondingly the faster of the pair. Likewise, alkene **3b** ($\Phi_T = 5.2(2)°$) is more twisted than **3d** ($\Phi_T = 2.8(1)°$), and is also the faster of the pair.

The Au−P bond lengths of gold complexes **2** are more or less constant and very close to the typical value (2.235 Å in Ph$_3$PAuCl).[20] The large atomic radius of gold engenders considerable steric congestion between the AuCl fragment and the aromatic moiety of the upper half in **2a** in particular, which manifests in an unusually large helical pitch compared to **2b−d** and a somewhat bent P−Au−Cl bond angle of 172.99(5)°. The P−O bond lengths in all of phosphine oxides **3a−d** are nearly equal and close to the typical value (~1.49 Å for Ph$_3$P=O).[21]

A "Shortcut" Isomerization Cycle Taking Advantage of Phosphorus Inversion. Finally, we note a unique feature of motor **1** in particular, which provides an unprecedented opportunity to regulate the rotary cycle. It is well known that trivalent phosphorus compounds can undergo pyramidal inversion, but the activation energy for this process is generally between 30 and 35 kcal/mol, so the rate is negligible near room temperature.[22,23] Indeed, although the chiral axes of motors **1a** and **1c** are configurationally stable at room temperature, they interconvert by pyramidal inversion at elevated temperatures to reach an equilibrium favoring isomer **1a** by a ca. 4:1 ratio at 100 °C (Scheme 2).[24] Eyring analysis gave a free energy of activation of $\Delta G^{\ddagger} = 28.2 \pm 1.3$ kcal/mol for the conversion of **1c** to **1a**, which is near the expected range for a triarylphosphine.

Because pyramidal inversion converts one diastereomer of stable helicity directly to the other stable diastereomer, it is possible to bypass half the conventional rotational cycle through this process. Thus, the configurational lability of the chiral axis of **1** at elevated temperatures enables a new rotational cycle that is
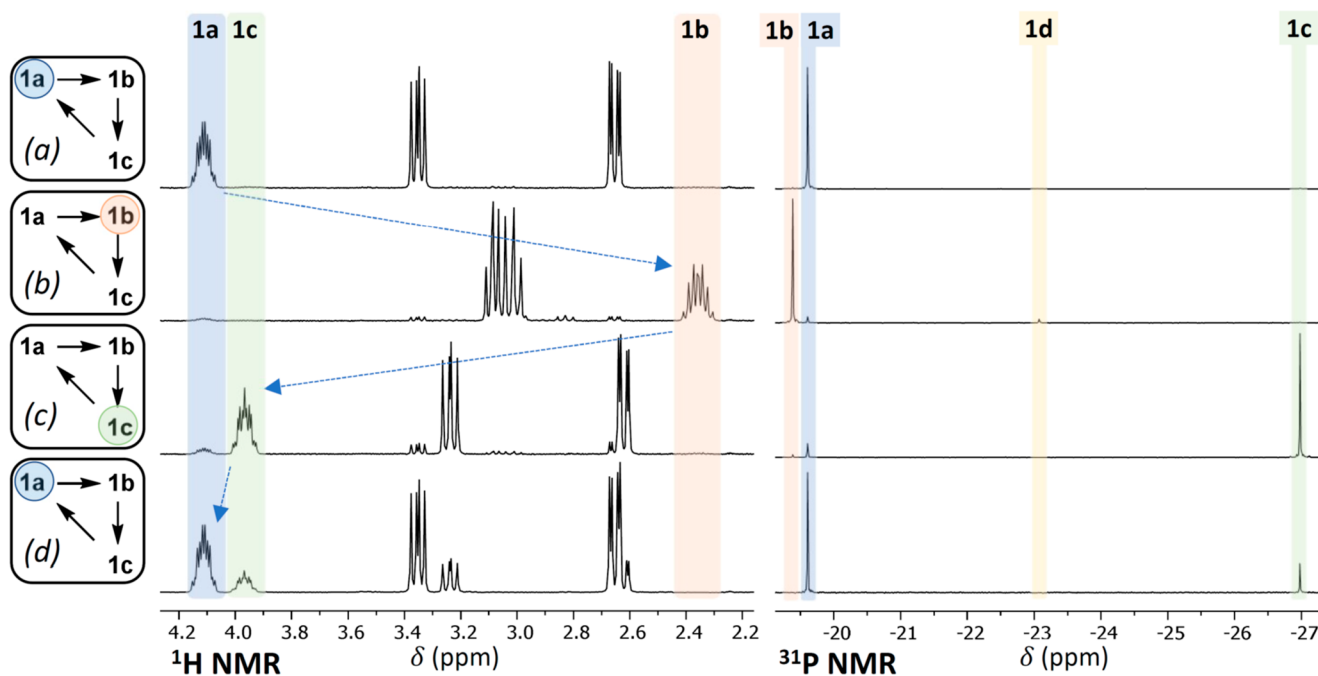
diastereomers, however, exhibit a substantially greater exocyclic bond angle C(2)−C(1)−C(15) on the side of the allylic methyl substituent (129.9° on average), which is compensated by a compression of only the endocyclic bond angle (107.0° on average). This deformation is attributable to greater nonbonded interactions in the less-stable isomers between the allylic methyl group and the proximal aromatic ring in the lower half: in the less-stable isomers, the allylic methyl group adopts a pseudo-equatorial position and unavoidably clashes with the lower half, while in the more stable isomers the methyl group is pseudo-axial.

All of the structures have some modest twisting about the central alkene double bond. Within each set of four diastereomers of motors **2** and **3**, the diastereomers of unstable helicity exhibit greater twisting than the stable diastereomers, as

Figure 8. A full transit through the "shortcut" cycle involving pyramidal inversion of motor **1**, monitored by ^{1}H and ^{31}P NMR. Top to bottom: (a) **1a** in d_8-toluene, (b) after irradiating with 365 nm light for 11 min at room temperature, (c) after subsequent heating at 42 °C for 36 h, and (d) after heating at 100 °C for 24 h.

unique among molecular motors: irradiation of **1a** leads predominantly to **1b**, THI of **1b** gives **1c** at modestly elevated temperature, and increasing the temperature further establishes an equilibrium favoring **1a**, which closes the cycle.

Figure 8 depicts one full transit through this novel isomerization cycle, as followed by ^{1}H and ^{31}P NMR. Starting from **1a** in rigorously degassed d_8-toluene solution (panel a), irradiation at 365 nm for 11 min at room temperature yields a mixture heavily favoring **1b** (**1a:b:c:d** = 4:92:3:<1), which is most readily discerned by the typical upfield shift of the allylic proton as it moves from a pseudo-equatorial position in **1a** to a pseudo-axial one in **1b** (panel b). Gentle heating of this mixture at 42 °C for 36 h converts **1b** completely to **1c** via THI (panel c). Finally, more vigorous heating at 100 °C for 24 h induces phosphorus inversion of **1c**, establishing an equilibrium favoring **1a** by nearly a factor of 4.

This unprecedented isomerization cycle is enabled by the unique element of axial chirality present in motors **1** and the semi-lability of the phosphorus center on which it is based. This novel concept could form the basis for the design of new molecular motors with a similar chiral axis but alternative, more facile modes of configurational inversion.

CONCLUSION

We have reported here the synthesis and characterization of three new second-generation molecular motors with unique axial chirality. We have shown for the first time that photochemical interconversion of all four diastereomeric states of such second-generation motors may be a rather general phenomenon, and experimental data supported by kinetic pathway calculations are consistent with all-photochemical unidirectional rotation. Finally, a unique three-stage photochemical−thermal−thermal isomerization cycle was found involving inversion of configuration of an axial chiral phosphorus stereoelement. Further work is aimed at precisely outlining the scope and uncovering the origin of this unusual behavior, and in particular elucidating the nature of the excited-state pathways at work.

ASSOCIATED CONTENT

Ⓢ Supporting Information

The Supporting Information is available free of charge at https://pubs.acs.org/doi/10.1021/jacs.0c08249.

> Experimental procedures, kinetic data, crystallography, kinetic modeling, and full characterization of all new compounds (PDF)

> Crystallographic data files, in CIF format, for **2a−d** and **3a−d** (ZIP)

AUTHOR INFORMATION

Corresponding Author

Ben L. Feringa − *Stratingh Institute for Chemistry, University of Groningen, 9747 AG Groningen, The Netherlands;* ⓞ orcid.org/0000-0003-0588-8435; Email: b.l.feringa@rug.nl

Authors

Gregory B. Boursalian − *Stratingh Institute for Chemistry, University of Groningen, 9747 AG Groningen, The Netherlands*

Eise R. Nijboer − *Stratingh Institute for Chemistry, University of Groningen, 9747 AG Groningen, The Netherlands*

Ruth Dorel − *Stratingh Institute for Chemistry, University of Groningen, 9747 AG Groningen, The Netherlands;* ⓞ orcid.org/0000-0002-8617-8648

Lukas Pfeifer − *Stratingh Institute for Chemistry, University of Groningen, 9747 AG Groningen, The Netherlands;* ⓞ orcid.org/0000-0002-8461-3909

Omer Markovitch − *Stratingh Institute for Chemistry and Groningen Institute for Evolutionary Life Sciences, University of Groningen, 9747 AG Groningen, The Netherlands; Origins Center, 9747 AG Groningen, The Netherlands;* ⓞ orcid.org/0000-0002-9706-5323

Alex Blokhuis − *Stratingh Institute for Chemistry and Groningen Institute for Evolutionary Life Sciences, University of Groningen, 9747 AG Groningen, The Netherlands*

Complete contact information is available at:
https://pubs.acs.org/10.1021/jacs.0c08249

ACKNOWLEDGMENTS

REFERENCES

(1) (a) Dattler, D.; Fuks, G.; Heiser, J.; Moulin, E.; Perrot, A.; Yao, X.; Giuseppone, N. Design of collective motions from synthetic molecular switches, rotors, and motors. *Chem. Rev.* **2020**, *120*, 310−433. (b) Sluysmans, D.; Stoddart, J. F. Growing Community of Artificial Molecular Machinists. *Proc. Natl. Acad. Sci. U. S. A.* **2018**, *115* (38), 9359. (c) Erbas-Cakmak, S.; Leigh, D. A.; McTernan, C. T.; Nussbaumer, A. L. Artificial Molecular Machines. *Chem. Rev.* **2015**, *115*, 10081. (d) *The Nature of the Mechanical Bond: From Molecules to Machines*; Bruns, C. J., Stoddart, J. F., Eds.; Wiley-VCH: Weinheim, 2016. (e) *Molecular Devices and Machines: Concepts and Perspectives for the Nanoworld*, 2nd ed.; Balzani, V., Credi, A., Venturi, M., Eds.; Wiley-VCH: Weinheim, 2008. (f) Browne, W. R.; Feringa, B. L. Making molecular machines work. *Nat. Nanotechnol.* **2006**, *1*, 25−35.

(2) (a) Garcia-Lopez, V.; Liu, D.; Tour, J. M. Light-Activated Organic Molecular Motors and Their Applications. *Chem. Rev.* **2020**, *120*, 79−124. (b) Baroncini, M.; Silvi, S.; Credi, A. Photo- and Redox-Driven Artificial Molecular Motors. *Chem. Rev.* **2020**, *120*, 200−268. (c) Roke, D.; Wezenberg, S. J.; Feringa, B. L. Molecular rotary motors: Unidirectional motion around double bonds. *Proc. Natl. Acad. Sci. U. S. A.* **2018**, *115*, 9423. (d) Petermayer, C.; Dube, H. Indigoid Photoswitches: Visible Light Responsive Molecular Tools. *Acc. Chem. Res.* **2018**, *51*, 1153−1163. (e) Kassem, S.; van Leeuwen, T.; Lubbe, A. S.; Wilson, M. R.; Feringa, B. L.; Leigh, D. A. Artificial Molecular Motors. *Chem. Soc. Rev.* **2017**, *46*, 2592. (f) Lubbe, A. S.; van Leeuwen, T.; Wezenberg, S. J.; Feringa, B. L. Designing dynamic functional

molecular systems. *Tetrahedron* **2017**, *73*, 4837–4848. (g) van Leeuwen, T.; Lubbe, A. S.; Stacko, P.; Wezenberg, S. J.; Feringa, B. L. Dynamic control of function by light-driven molecular motors. *Nat. Chem. Rev.* **2017**, *1*, 0096.

(3) (a) Danowski, W.; van Leeuwen, T.; Abdolahzadeh, S.; Roke, D.; Browne, W. R.; Wezenberg, S. J.; Feringa, B. L. Unidirectional rotary motion in a metal-organic framework. *Nat. Nanotechnol.* **2019**, *14*, 488–494. (b) Danowski, W.; Castiglioni, F.; Sardjan, A. S.; Krause, S.; Pfeifer, L.; Roke, D.; Comotti, A.; Browne, W. R.; Feringa, B. L. Visible-Light-Driven Rotation of Molecular Motors in a Dual-Function Metal–Organic Framework Enabled by Energy Transfer. *J. Am. Chem. Soc.* **2020**, *142*, 9048–9056. (c) Castiglioni, F.; Danowski, W.; Perego, J.; Leung, F. K.-C.; Sozzani, P.; Bracco, S.; Wezenberg, S. J.; Comotti, A.; Feringa, B. L. Modulation of porosity in a solid material enabled by bulk photoisomerization of an overcrowded alkene. *Nat. Chem.* **2020**, *12*, 595–602.

(4) Chen, J.; Leung, F. K.-C.; Stuart, M. C. A.; Kajitani, T.; Fukushima, T.; van der Giessen, E.; Feringa, B. L. Artificial muscle-like function from hierarchical supramolecular assembly of photoresponsive molecular motors. *Nat. Chem.* **2018**, *10*, 132–138. (b) Leung, F. K.-C.; van den Enk, T.; Kajitani, T.; Chen, J.; Stuart, M. C. A.; Kuipers, J.; Fukushima, T.; Feringa, B. L. Supramolecular Packing and Macroscopic Alignment Controls Actuation Speed in Macroscopic Strings of Molecular Motors Amphiphiles. *J. Am. Chem. Soc.* **2018**, *140*, 17724–17733.

(5) Eelkema, R.; Pollard, M. M.; Vicario, J.; Katsonis, N.; Ramon, B. S.; Bastiaansen, C. W. M.; Broer, D. J.; Feringa, B. L. Nanomotor rotates microscale objects. *Nature* **2006**, *440*, 163.

(6) Gerwien, A.; Mayer, P.; Dube, H. Photon-Only Molecular Motor with Reverse Temperature-Dependent Efficiency. *J. Am. Chem. Soc.* **2018**, *140*, 16442–16445.

(7) (a) Koumura, N.; Geertsema, E. M.; Meetsma, A.; Feringa, B. L. Light-Driven Molecular Rotor: Unidirectional Rotation Controlled by a Single Stereogenic Center. *J. Am. Chem. Soc.* **2000**, *122*, 12005–12006. (b) Koumura, N.; Geertsema, E. M.; van Gelder, M. B.; Meetsma, A.; Feringa, B. L. Second Generation Light-Driven Molecular Motors. Unidirectional Rotation Controlled by a Single Stereogenic Center with Near-Perfect Photoequilibria and Acceleration of the Speed of Rotation by Structural Modification. *J. Am. Chem. Soc.* **2002**, *124*, 5037–5051. (c) Feringa, B. L. In Control of Motion: From Molecular Switches to Molecular Motors. *Acc. Chem. Res.* **2001**, *34*, 504–513.

(8) Eliel, E. L.; Wilen, S. H. *Stereochemistry of Organic Compounds*; John Wiley & Sons, Inc.: New York, 1994; pp 1133–1138.

(9) (a) Schaub, T. A.; Brülls, S. M.; Dral, P. O.; Hampel, F.; Maid, H.; Kivala, M. Organic Electron Acceptors Comprising a Dicyanomethylene-Bridged Acridophosphine Scaffold: The Impact of the Heteroatom. *Chem. - Eur. J.* **2017**, *23*, 6988–6992. (b) Gray, M.; Chapell, B. J.; Taylor, N. J.; Snieckus, V. Carbanion-Mediated Heterocyclizations: Regiospecific, General Route to Dibenzo[b,e]-phosphininones by Synthetic Anionic Equivalents of Friedel-Crafts Reactions and Remote Fries Rearrangement. *Angew. Chem., Int. Ed. Engl.* **1996**, *35*, 1558–1560.

(10) For studies of photochemical isomerization of alkylidinecycloalkanes, see: (a) Lemieux, R. P.; Schuster, G. B. Photochemistry of axially chiral (arylmethylene)cycloalkanes: a search for suitable photoswitchable liquid crystalline materials. *J. Org. Chem.* **1993**, *58*, 100–110. (b) Zhang, Y.; Schuster, G. B. Photoresolution of an Axially Chiral Bicyclo[3.2.1]octan-3-one: Phototriggers for a Liquid Crystal-Based Optical Switch. *J. Org. Chem.* **1995**, *60*, 7192–7197. (c) Suarez, M.; Schuster, G. B. Photoresolution of an Axially Chiral Bicyclo[3.3.0]-octan-3-one: Phototriggers for a Liquid-Crystal-Based Optical Switch. *J. Am. Chem. Soc.* **1995**, *117*, 6732–6738.

(11) Kulago, A. A.; Mes, E. M.; Klok, M.; Meetsma, A.; Brouwer, A. M.; Feringa, B. L. Ultrafast Light-Driven Nanomotors Based on an Acridane Stator. *J. Org. Chem.* **2010**, *75*, 666–679.

(12) Although we were able to obtain X-ray crystal structures of all four diastereomeric states of motors **2** and **3**, obtaining suitable crystals of the unstable states **2b**, **2d**, **3b**, and **3d** was quite challenging, and required several attempts and careful crystal selection in almost every case. All attempts to isolate the unstable diastereomers by preparative recrystallization from mixtures obtained through irradiation of stable isomers failed due to co-crystallization of the other diastereomers in the mixture.

(13) Maafi, M.; Maafi, W. Modeling and Elucidation of the Kinetics of Multiple Consecutive Photoreactions AB$_4$(4Φ) With Φ-order Kinetics. Application to the Photodegradation of Riboflavin. *J. Pharm. Sci.* **2016**, *105*, 3537–3548.

(14) (a) Espenson, J. H. *Chemical Kinetics and Reaction Mechanisms*, 2nd ed.; McGraw-Hill: New York, 1995; p 72. (b) Szabó, Z. G. Kinetic Characterization of Complex Reaction Systems. In *Comprehensive Chemical Kinetics*. Bramford, C. H., Tipper, C. F. H., Eds.; Elsevier: Amsterdam, 1969; Vol. 2, pp 17–35.

(15) In the low absorption regime, in which the absorbance at the wavelength of irradiation remains small throughout the reaction, the photokinetic factor can be considered constant to a good approximation (see ref 16). Because motors **2** and **3** scarcely absorb at their respective irradiation wavelengths, the errors engendered by our approach should be small.

(16) Mauser, H.; Gauglitz, G. Photokinetics: Theoretical Fundamentals and Applications. In *Comprehensive Chemical Kinetics*; Compton, R. G., Hancock, G., Eds.; Elsevier: Amsterdam, 1998; Vol. 36, p 200.

(17) Pijper, D.; Jongejan, M. G. M.; Meetsma, A.; Feringa, B. L. Light-Controlled Supramolecular Helicity of a Liquid Crystalline Phase Using a Helical Polymer Functionalized with a Single Chiroptical Molecular Switch. *J. Am. Chem. Soc.* **2008**, *130*, 4541–4552.

(18) Crystallographic characterization of all four diastereomeric states has been accomplished for a different kind of molecular motor based on hemithioindigo; see ref 6.

(19) For a review of structural trends in strained alkenes, see: Luef, W.; Keese, R. Strained Olefins: Structure and Reactivity of Nonplanar Carbon–Carbon Double Bonds. In *Topics in Stereochemistry*; Eliel, E. L., Wilen, S. H., Eds.; John Wiley and Sons: New York, 1991; Vol. 20, pp 231–318.

(20) Baenziger, N. C.; Bennett, W. E.; Soborofe, D. M. Chloro-(triphenylphosphine)gold(I). *Acta Crystallogr., Sect. B: Struct. Crystallogr. Cryst. Chem.* **1976**, *32*, 962.

(21) Gilheany, D. G. Structure and Bonding in Tertiary Phosphine Chalcogenides. In *The Chemistry of Organophosphorus Compounds, Vol. 2, Phosphine Oxides, Sulphides, Selenides and Tellurides*; Hartley, F. R., Ed.; John Wiley & Sons: New York, 1992; pp 1–52.

(22) Baechler, R. D.; Mislow, K. Effect of structure on the rate of pyramidal inversion of acyclic phosphines. *J. Am. Chem. Soc.* **1970**, *92*, 3090–3093.

(23) For general reviews on the pyramidal inversion phenomenon of phosphorus and other elements, see: (a) Rauk, A.; Allen, L. C.; Mislow, K. Pyramidal Inversion. *Angew. Chem., Int. Ed. Engl.* **1970**, *9*, 400. (b) Mislow, K. Pyramidal Inversion Barriers of Phosphines and Arsines. *Trans. N. Y. Acad. Sci.* **1973**, *35*, 227.

(24) To the best of our knowledge, inversion of a chiral axis through pyramidal inversion at phosphorus is unprecedented. The only known organophosphorus compounds with an axial stereoelement similar to motors **1** are a few 1-alkyl-4-(alkylidine)phosphorinanes, though no study of their inversion has been reported to our knowledge. See: (a) Quin, L. D.; Shook, H. E., Jr Attempted conversion of 1-alkyl-4-(2-hydroxyethyl)-4-phosphorinanols into bicyclic phosphonium salts by a quinuclidine synthesis. *J. Org. Chem.* **1967**, *32*, 1604–1607. (b) Quin, L. D.; Russell, J. W.; Prince, R. D.; Shook, H. E., Jr Double-bond migration in 1-methyl-4-(carbethoxymethylene)phosphorinane. *J. Org. Chem.* **1971**, *36*, 1495–1499.